REVIEW PAPER

CrossMark

Bacterial Ferrihydrite Nanoparticles: Preparation, Magnetic Properties, and Application in Medicine

S. V. Stolyar[1,2] · D. A. Balaev[1,3] · V. P. Ladygina[2] · A. A. Dubrovskiy[3] · A. A. Krasikov[3] · S. I. Popkov[1,3] · O. A. Bayukov[3] ·
Yu V. Knyazev[3] · R. N. Yaroslavtsev[1,3] ⬤ · M. N. Volochaev[3] · R. S. Iskhakov[3] · K. G. Dobretsov[4] · E. V. Morozov[2,3] ·
O. V. Falaleev[2,3] · E. V. Inzhevatkin[2] · O. A. Kolenchukova[5] · I. A. Chizhova[1]

Abstract

Nanoparticles of antiferromagnetically ordered materials acquire the uncompensated magnetic moment caused by defects and surface effects. A bright example of such a nano-antiferromagnet is nanoferrihydrite consisting of particles 2–5 nm in size, the magnetic moment of which amounts to hundreds of Bohr magnetons per particle. We present a brief review of the studies on magnetic properties of ferrihydrite produced by bacteria. Special attention is focused on the aspects of possible biomedical applications of this material, i.e., the particle elimination, toxicity, and possible use for targeted drug delivery.

1 Introduction

The materials containing magnetic nanoparticles are interesting both for fundamental research concerning the drastic difference of their magnetic properties from those of bulk analogs and for application in various fields [1, 2]. It is well known that as the size of ferro- and ferrimagnetic particles decreases, surface atoms start playing a decisive role in the magnetic state formation. This often leads to a decrease in the saturation magnetization of a nanostructured material due to the break of chemical bonds and spin-glass state of surface atoms [3]. As a result, magnetic moment (μ_P) of ferro- and ferrimagnetic nanoparticles decreases with particle size (d) much faster than the quantity proportional to particle volume (V) ($V \sim d^3$) [3–5].

✉ R. N. Yaroslavtsev
yar-man@bk.ru

[1] Siberian Federal University, Krasnoyarsk, Russia

[2] Krasnoyarsk Scientific Center, Federal Research Center KSC SB RAS, Krasnoyarsk, Russia

[3] Kirensky Institute of Physics, Federal Research Center KSC SB RAS, Krasnoyarsk, Russia

[4] Siberian Clinical Center, FMBA, Krasnoyarsk, Russia

[5] Scientific Research Institute of Medical Problems of the North, Federal Research Center KSC SB RAS, Krasnoyarsk, Russia

In the antiferromagnetically ordered nanoparticles, the surface effects and defects in the bulk of particles play a fundamentally different role: these particles acquire uncompensated magnetic moment (μ_{unc}, $\mu_P = \mu_{unc}$), the value of which depends on the particle size and defect type. Based on the statistical considerations, Néel proposed the interrelation between the number of atoms (N) in a particle (obviously, $N \sim V$), uncompensated magnetic moment (μ_{unc}), and defect type [6].

$$\mu_{unc} \sim \mu_{at} N^b \tag{1}$$

where μ_{at} is the magnetic moment of a magnetically active atom and b is the exponent that takes the value of 1/3, 1/2, or 2/3 for defects on the surface and in the bulk of a particle or the odd number of ferromagnetically ordered planes in a particle. Indeed, according to the data reported in [2, 7–15], (1) is valid for antiferromagnetic (AFM) nanoparticles of different compositions. This gives grounds for studying the fundamental properties of AFM nanoparticles and opens the opportunities for their application, e.g., in medicine, due to the fact that an AFM particle of a few nanometers in size can have a magnetic moment comparable with that of a ferro- or ferrimagnetic particle. Ferrihydrite with the nominal chemical formula $5Fe_2O_3 \cdot 9H_2O$ (the number of OH bonds and water content can change under the action of structural defects) stands out from the diversity of antiferromagnetically ordered nanoparticle types. This mineral exists in the nanosized form in almost all living

organisms and works as an iron repository, being a part of the so-called ferritin. Ferritin extracted from a horse spleen was thoroughly investigated [7, 10, 14, 15]. It was established that the μ_{unc} value for ferritin with a ferrihydrite core ~ 5 nm in size amounts to several Bohr magnetons (μ_B).

Ferrihydrite nanoparticles can be obtained using chemical methods [16, 17] or by extracting the products of bacterial vital activity. One of the techniques for preparing bacterial ferrihydrite is based on cultivation of *Klebsiella oxytoca* bacteria from lake sediments [18, 19]. This study presents a brief review of the investigations of the magnetic properties of bacterial ferrihydrite nanoparticles; the possibility of targeted particle coarsening by heat treatment [20, 21] and, as a consequence, the modification of the magnetic properties of this material; peculiarities of magnetic hysteresis; and some results of the clinical examination of laboratory animals with the use of ferrihydrite nanoparticles.

2 Preparation and Characterization of Biogenic Ferrihydrite Nanoparticles

The *Klebsiella oxytoca* strain used for producing ferrihydrite was extracted from the sapropel of the Borovoe Lake, Krasnoyarsk territory. Microorganisms were inoculated into an agar medium and grown under anaerobic conditions. After multiple ultrasonic processing of bacterial sediments, centrifugation, and washing, a stable sol of nanoparticles in an aqueous solution was fabricated and dried. The obtained powder of magnetic nanoparticles is hereinafter referred to as as-prepared sample. Note that as-prepared samples of different sets demonstrated similar characteristics. A part of the powder was kept in air at temperatures within the range of 150–200 °C for different times.

X-ray diffraction patterns of the prepared samples are characteristic of the amorphous state. The ferrihydrite nanoparticles were characterized by Mössbauer spectroscopy. According to the Mössbauer spectra, iron atoms

in bacterial ferrihydrite can occupy three sites with different quadrupole splittings characteristic of ferrihydrite [18, 20, 22]. The results of analysis of Mössbauer spectra are mainly identical for as-prepared samples of different sets. The formation of new iron oxide phases in bacterial ferrihydrite upon annealing was not observed [13, 20].

Typical transmission electron microscopy (TEM) data for the as-prepared ferrihydrite sample are shown in Fig. 1. The average ferrihydrite nanoparticle size $<d>$ estimated from several micrographs was found to be ~ 2.7 nm. The low-temperature heat treatment leads to the increase in the particle size (the $<d>$ value of the sample treated at 150 °C for 24 h is ~ 4 nm).

3 Magnetic Properties of Bacterial Ferrihydrite Nanoparticles and Their Transformation upon Low-Temperature Heat Treatment

3.1 The Superparamagnetic Behavior of Bacterial Ferrihydrite Nanoparticles, the Origin of Uncompensated Magnetic Moment, and the Effect of Low-Temperature Heat Annealing

Figure 2 presents typical temperature dependences of the magnetic moment ($M(T)$) obtained upon cooling the ferrihydrite samples annealed for different times at temperatures of 150 and 200 °C in the nonzero (FC) and nonzero (ZFC) external field modes. The difference between the $M(T)_{ZFC}$ and $M(T)_{FC}$ dependences and the pronounced maximum in the $M(T)_{ZFC}$ dependences evidence for the superparamagnetic (SP) behavior of the investigated particles. In addition, according to our data, the maximum temperature (hereinafter, blocking temperature, T_B) shifts toward lower temperatures, which is typical of the SP systems. Note that for the as-prepared ferrihydrite samples from different series, the T_B value in the same field differed by no more than 3 °C and lied between 23 and 25 K ($H = 1$ kOe). In addition, it can be seen in Fig. 2 that

Fig. 1 Typical TEM micrographs obtained using a Hitachi HT7700 facility. **a** FH (as-prepared). **b** FH (annealed for 24 h)

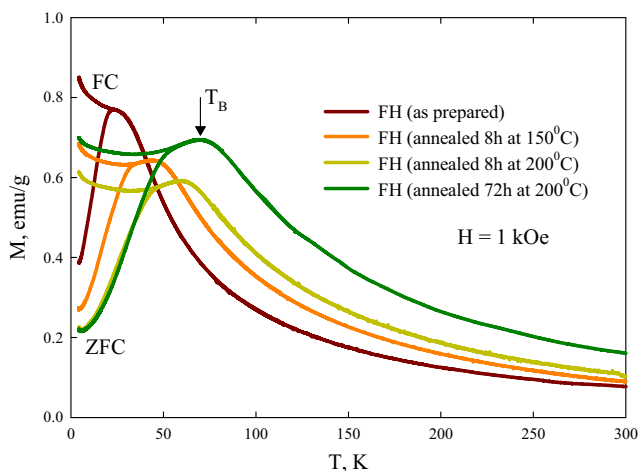(a) 0h

FH (as-prepared)

FH (annealed for 24 h)
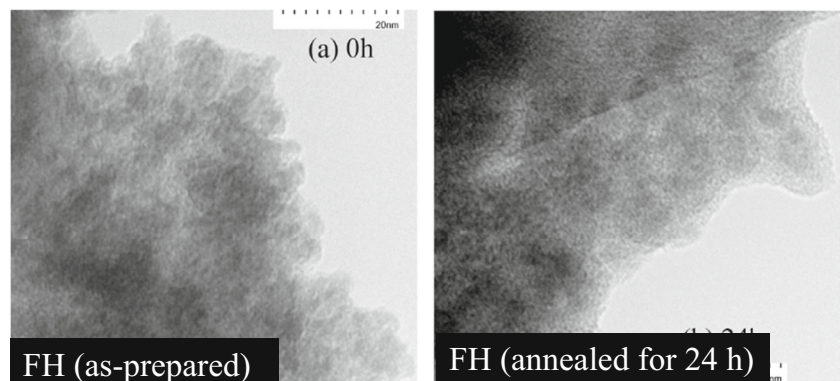
Fig. 2 FC and ZFC $M(T)$ dependences for the as-prepared and annealed ferrihydrite samples

annealing significantly increases the blocking temperature and this effect is governed by the annealing temperature and time.

Based on the classical Néel–Brown relation

$$kT_B = K_{eff}V/\ln(\tau/\tau_0) \approx K_{eff}V/25 \qquad (2)$$

where k is the Boltzmann constant, K_{eff} is the effective magnetic anisotropy constant, V is the particle volume, and τ and $\tau_0 \sim 10^{-9} - 10^{-10}$ s are the characteristic times of the measurements ($\tau \sim 10^2$ s for the magnetic measurements) and particle relaxation, respectively, and we may conclude that the annealing increases the particle size. This is confirmed by the TEM data (Fig. 1).

The particle size growth during annealing is confirmed also by the magnetization curves ($M(H)$) in the temperature range of $T > T_B$. Figure 3 shows magnetization isotherms for the as-prepared samples and the samples annealed at 160 °C for 24 h. According to the generally accepted approach, the magnetization curve of the ensemble of AFM

nanoparticles in the region of $T > T_B$ can be described by the expression

$$M(H) = N_P \int_0^\infty L(\mu_P, H) f(\mu_P) \mu_P d\mu_P + \chi_{AF} \times H. \qquad (3)$$

This expression was written with regard to the distribution over magnetic moments ($f(\mu_P)$). The first term of (3) describes the alignment of particle magnetic moments (μ_P) along the external field direction in accordance with the classical Langevin function $L(\mu_P, H)(L(\mu_P, H) = \coth(\mu_P \times H/kT) - 1/(\mu_P \times H/kT))$; N_P is the number of particles in unit mass. The second term $\chi_{AF} \times H$ describes the "cant" of sublattices of the AFM particle core (χ_{AF} is the AFM susceptibility of the particle core). Solid lines in Fig. 3 show the best fitting of the experimental data by (3) using the lognormal distribution over the magnetic moments: $f(\mu_P) = (\mu_P \cdot s \cdot (2\pi)^{1/2})^{-1} \exp\{-[\ln(\mu_P/n)]^2/2s^2\}$, where $<\mu_P> = n \cdot \exp(s^2)$ is the average particle magnetic moment and s^2 is the $\ln(\mu_P)$ dispersion.

The inset in Fig. 3b illustrates the temperature behavior of $<\mu_P>$, which is described well by the law $<\mu_P(T)> = <\mu_P(T = 0)> \times (1 - T^a)$ at typical a values between 1.5 and 2.0. It can be seen that annealing leads to a noticeable increase in $<\mu_P>$. This allows us to reliably determine the $<\mu_P>$ value from the $M(H)$ data at $T = 0$ for the as-prepared and annealed samples (162 and 302 μ_B, respectively). These values correspond to the numbers of uncompensated iron atoms of ~ 30 and ~ 60 (at $\mu_{Fe^{3+}} = 5\ \mu_B$) and agree well with the model Néel hypothesis with the exponent $b \approx 1/2$ in (1). Indeed, using the values of $<d> \approx 2.7$ nm for the as-prepared sample and ~ 4.0 nm for the annealed sample (Fig. 1 shows the data for this sample series) and taking an average distance of 0.31 nm between Fe atoms in ferrihydrite [9], we obtain the numbers of iron atoms of $N \sim 600$ and 2200 in the approximation of the cubic particle shape and, consequently, $N^{1/2} \approx 25$ and ≈ 47. Thus, the uncompensated magnetic moment of

Fig. 3 **a**, **b** Experimental (dots) and fitting (lines, (3) $M(H)$ dependences for the ferrihydrite samples. The inset on the left shows the temperature behavior of fitting parameter $<\mu_P>$
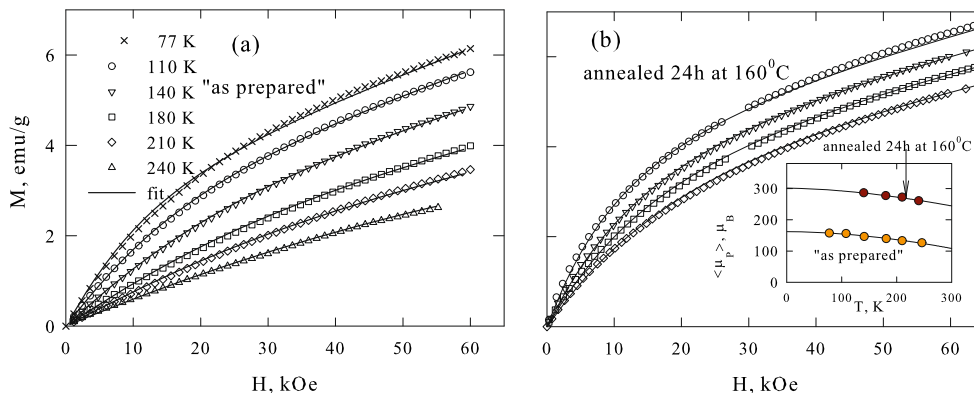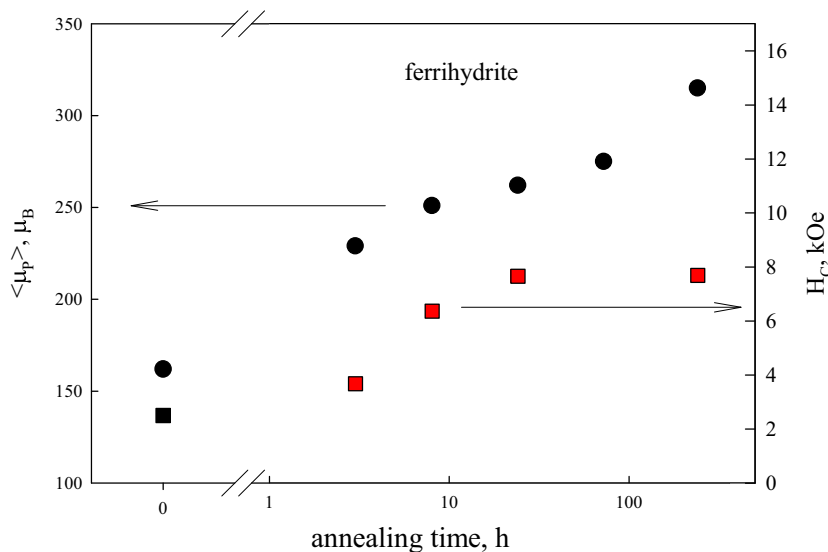
the bacterial ferrihydrite occurs due to defects both on the surface and in the bulk of a sample.

The dependence of the quantity $<\mu_P(T = 0)>$ on annealing time is illustrated in Fig. 4. It seems reasonable to explain the particle coarsening upon annealing by the agglomeration of neighboring particles [20, 21]; note that at higher temperatures, ferrihydrite decomposes with the formation of the hematite phase [22]. One may conclude that low-temperature annealing on air is the effective way to change the size as well as magnetic properties (the blocking temperature, the value of uncompensated magnetic moment) of ferrihydrite nanoparticles. Recently, it was shown that low-temperature annealing of *chemical* ferrihydrite also results in an increase of the particle size of this nanomaterial [23].

3.2 Peculiarities of Magnetic Hysteresis in the Blocked State and Hysteresis Loop Shift upon Cooling in an External Field from the Unblocked State

Within the temperature range $T < T_B$, the isotherms of magnetization ($M(H)$) of ferrihydrite nanoparticles are hysteretic. At $T = 4.2$ K, the value of coercivity (H_C, obtained from $M(H)$ curves measured at the maximal applied field, $H_{max} = \pm 60$ kOe) lies within 1.5–3.0 kOe for as-prepared samples from different series. Low-temperature annealing results to enhancement of coercivity at $T = 4.2$ K; see Fig. 4. This behavior can be understood, taking into account the Stoner-Wohlfarth expression for single-domain particles: $H_C \approx \frac{K_{eff}}{M_S}[1 - (T/T_B)^{1/2}]$, where M_S is the saturation magnetization [24]. Indeed, $M_S = \mu_P/V$ and $\mu_P \sim N^{1/2} \sim V^{1/2}$; therefore, $M_S \sim V^{-1/2}$ and $H_C \sim V^{1/2}$; i.e., coercivity increases with the growth of particle size (increases with annealing time).

On the other hand, AF nanoparticles are known to exhibit a very high irreversibility field of magnetization hysteresis [7, 9, 13, 14, 20, 21, 25]. Therefore, in most cases, the $M(H)$ hysteretic dependences are partial [15, 25]. Also, many authors observed a shift of hysteresis loop on systems of AF nanoparticles after cooling them in a magnetic field from a temperature which is higher than the blocking temperature [7, 9, 13, 15, 25–35] (FC conditions). However, it is questionable whether the shift of $M(H)$ hysteresis is due to an internal effect (exchange bias) or is an analogue of the minor loop effect after field cooling [15]. Here, we show a method, which allows to separate these effects.

An example of ZFC $M(H)$ hysteresis dependence obtained by cycling external field up to its maximal values (H_{max}) with a gradual increase in the H_{max} is shown in Fig. 5. $M(H)$ curves measured after field cooling at $H = 30$ kOe are also shown in this figure. Figure 6 shows the H_C values as a function of maximal applied field (H_{max}) deduced from $M(H)$ data (from Fig. 5) for ZFC case. It is seen that $H_C(H_{max})$ dependence has a tendency to saturate. Authors [15] argued that this dependence can be described by the following expression:

$$H_C(H_{max}) = H_{Cinf}[1 - (H^*/H_{max})^\beta] \tag{4}$$

where H_{Cinf} is the "infinite coercivity" (i.e., the H_C value at very high H_{max}). Equation (4) is valid at the fields higher than H^*, and the exponent β is determined by the structure of energy barriers of which the particle moment (μ_P) overcomes during the magnetization process [15]. Experimental data ($H_C(H_{max})$) are well described by (4) within the range $H > 30$ kOe at $\beta = 1.5$, $H^* = 19$ kOe, and $H_{Cinf} \approx 3.7$ kOe. The magnitude of H_{Cinf} is shown in Fig. 6 as horizontal dashed line.

Fig. 4 Average magnetic moment $<\mu_P(T = 0)>$ of ferrihydrite particles (left scale) and coercivity (H_C, at $T = 4.2$ K and $H_{max} = 60$ kOe) vs time of annealing at 160 °C
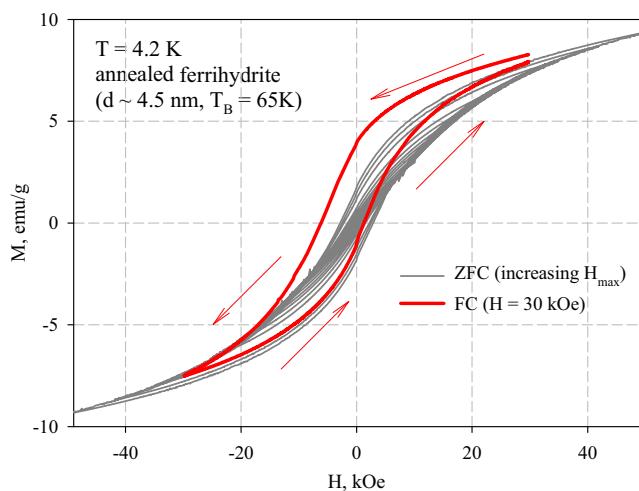
Fig. 5 ZFC hysteresis loops at $T = 4.2$ K together with the FC hysteresis loop at the cooling field 30 kOe for the ferrihydrite sample. For ZFC hysteresis loops, the external field is cycling up its maximal values ($\pm H_{max}$) with a gradual increase in the H_{max}. Arrows indicate the direction of the variation in external field for the FC hysteresis loop

Also, pairs of points at abscissa $H = 15$ kOe and $H = 30$ kOe in Fig. 6 are the values of "left" H_{CL} and "right" H_{CR} coercivity obtained for $M(H)$ hysteresis after cooling in these fields. It is seen from Fig. 6 that the "left" FC $|H_{CL}|$ values noticeably exceed the magnitude of $|H_{Cinf}|$. This supports that the observed shift of $M(H)$ loop after field cooling is due to the internal effect (not the minor loop effect). On the other hand, the difference $|H_{CL} - H_{CR}|$ is dependent on the cooling field. This behavior can be considered as a manifestation of another mechanism,
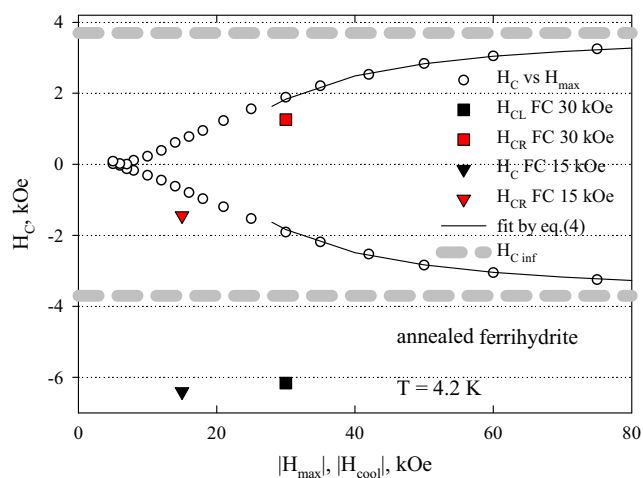
namely the minor loop effect. This effect reveals when after field cooling at some H_{cool} value and changing the field to the negative value ($-H_{cool}$), the field is further cycled until $\pm H_{cool}$ values are obtained. Therefore, the magnitude of loop shift (or exchange bias field, H_{SH}) is determined by an H_{CL} value and can be obtained as follows: $H_{SH} = |H_{CL}| - |H_{Cinf}|$ [25]. Figure 7 shows a variation of H_{SH} as a function of particle size $<d>$ for a series of as-prepared and annealed ferrihydrite samples.

As can be seen from Fig. 7, the H_{SH} magnitude grows monotonously with the particle size and the loop shift is not observed for ferrihydrite nanoparticles whose size is less than 3 nm. An increase of the loop shift with the particle size was observed on CuO and NiO nanoparticles [29, 30], while at a certain size (~ 26 nm for NiO [29] and 12 nm for CuO [30]), a subsequent decrease in H_{EB} at larger sizes was detected.

There are at least two possible mechanisms of loop shift in AFM nanoparticles. The first mechanism is exchange bias which is known to take place in FM/AFM (FM is ferro- or ferrimagnet) structures (films) or core-shell nanoparticles [1]. In the case of "pure" AF nanoparticles, there is a possibility of exchange coupling between the uncompensated magnetic moment (μ_P) (FM) and AF "core" of a particle. The second mechanism was pointed out by Kodama and Berkowitz [3]; they have shown that the existence of a large number of the broken exchange bonds on the surface can lead to the occurrence of the multi-sublattice states in an AF nanoparticle and this may result to the shift of $M(H)$ loop after field cooling. Further studies of the temperature behavior of H_{SH}, possibly, allow determination of the main mechanism responsible to the loop shift after FC conditions in ferrihydrite.

Fig. 6 Dependences of coercivity (H_C) on the maximal applied field H_{max} for the annealed ferrihydrite sample (mean size $<d> \sim 4.5$ nm) obtained from the ZFC hysteresis loops at 4.2 K (see Fig. 5). Solid lines indicate the best fittings by (4) for obtaining the "infinite coercivity" H_{Cinf} value shown by the horizontal dashed lines. The data on H_{CL} and H_{CR} for the FC hysteresis loops are built at the abscissas corresponding to the cooling field (30 and 60 kOe)
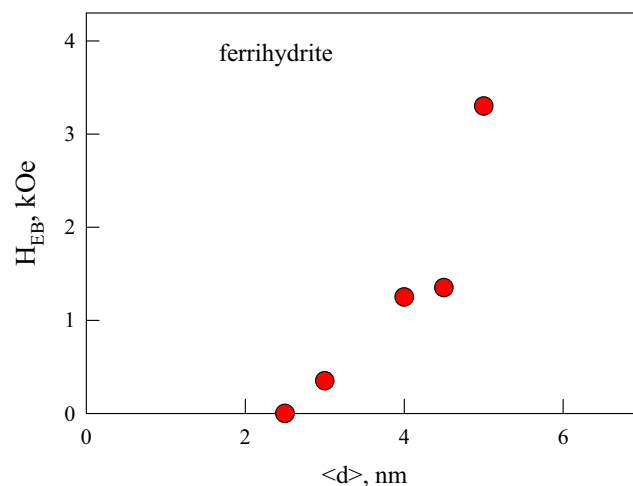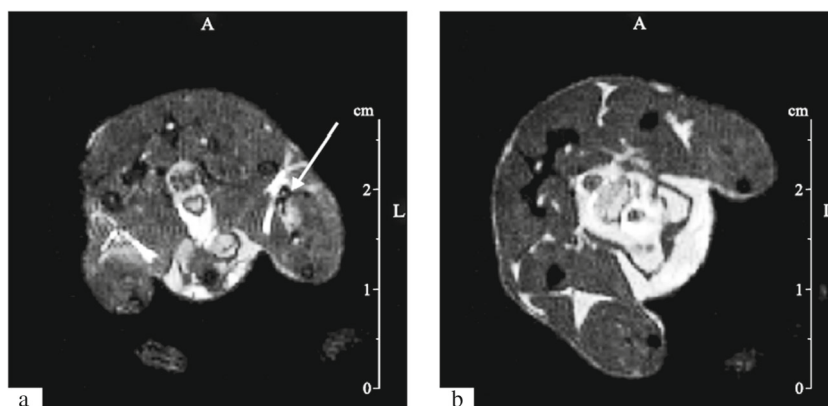

Fig. 7 Dependence of the loop shift (obtained by expression $H_{SH} = |H_{CL}| - |H_{Cinf}|$, see Fig. 6) after field cooling as a function of particle size for a series of the annealed ferrihydrite samples

Fig. 8 **a**, **b** Tomography images of the thigh cross section in 15 min and 2 h after the intramuscular injection of the suspension of ferrihydrite nanoparticles

4 Possible Applications in Medicine

4.1 Elimination of Ferrihydrite Nanoparticles from the Organism

Elimination of ferrihydrite nanoparticles from the organism was studied by NMR tomography on laboratory animals (mice). The suspension containing 0.7 g/l H_2O was injected singly abdominally in an amount of 1 ml or singly intramuscularly in a thigh in an amount of 0.1 ml.

The tomography study was carried out on a Bruker Avance DPX 200 NMR facility in a field of 4.7 T with a Greate 3/60 gradient block. The ^1H nuclear tomographic images were obtained by a spin-echo technique [36].

Figure 8 shows typical tomographic images of the thigh cross section in 15 min and 2 h after the intramuscular injection of the suspension. For a time period of 15 min, the signal intensity noticeably increases (shown by the arrow in Fig. 8a), which is reasonable to attribute to the presence of magnetic nanoparticles. However, for a period of 2 h, we noticed no changes in the signal intensity within the sensitivity of the method (10 μg per 1 g of tissue). These results were obtained also for the cross-sectional peritoneal cavity images after the abdominal drug injection. Based on the results obtained, we may conclude that ferrihydrite nanoparticles can be eliminated, at least, at the intramuscular and abdominal injection.

4.2 Targeted Drug Delivery and Nontoxicity of Ferrihydrite NPs

To establish the possibility of targeted drug delivery and the effect of magnetic nanoparticles on the conditions of inflammatory and reparative processes of laboratory animals, we compared the results of the treatment of three groups of animals (rats). The animals of group I were not treated, the animals of group II were treated by ampicillin, and the animals of group III were treated by ampicillin (500 mg) combined with ferrihydrite nanoparticles. The thermal injury region was affected by an external magnetic field (Polyus-101, magnetic field gradient of 4–6 mT/mm, and magnetic induction of 10–20 mT) for 20 min.

Macroscopic control of the reparative process of burnt rats showed that in the group of animals treated locally by ampicillin with nanoparticles, the wound healing occurred twofold faster than in the group of animals treated by pure ampicillin (Fig. 9).

The cytological examination of thermal injury smears showed that during the first day after the burn, all animals experienced the degenerative inflammatory changes. The local use of ampicillin with nanoparticles in group III significantly reduced the inflammation and activated the tissue regeneration, which was reflected in the regenerative inflammatory cytogram type.

Fig. 9 Thermal injury of rats treated by **a** ampicillin and **b** ampicillin with magnetic nanoparticles in 7 days

Comparative analysis of the microflora of the rats treated by ampicillin showed that the *Staphylococcus* bacteria on the thermal injury surface retained their content [37]. The situation was opposite in the group of rats treated by ampicillin with magnetic nanoparticles. The amount of *Staphylococcus* bacteria was much smaller.

5 Conclusions

The nanoparticles of biogenic ferrihydrite obtained from the *Klebsiella oxytoca* bacterial vital products have the uncompensated magnetic moment caused by defects on the surface and in the bulk of the particles. The presence of a magnetic moment of particles leads to the characteristic SP behavior. The described procedure yields nanoparticles ~ 3 nm in size with an SP blocking temperature of ~ 23–25 K and an average particle magnetic moment $<\mu_\mathrm{P}>$ of 150–200 μ_B. Heat treatment in air at 150–200 °C increases the T_B and $<\mu_\mathrm{P}>$ values due to the particle coarsening via agglomeration. In the low temperature range ($T < T_\mathrm{B}$), the magnetization curve of ferrihydrite samples is hysteretic with a typical value of coercivity (H_C) ~ 3–10 kOe (the H_C value increases upon annealing). Also, ferrihydrite particles over 3 nm in size (or with the T_B value higher than 40 K) exhibit the magnetic hysteresis loop shift after cooling in an external magnetic field starting from the temperature higher than T_B.

According to the NMR study, elimination of ferrihydrite nanoparticles at the intermuscular and abdominal injection occurs for the time of no longer than 2 h. The positive results of using the drugs in combination with nanoparticles for treating thermal injuries under the action of a gradient magnetic field together with ferrihydrite nontoxicity open wide opportunities for application of these nanoparticles in biomedicine.

References

1. Nogués, J., Sort, J., Langlais, V., Skumryev, V., Suriñach, S., Muñoz, J.S., Baró, M.D.: Exchange bias in nanostructures. Phys. Rep. **422**, 65–117 (2005)

2. Mørup, S., Madsen, D.E., Frandsen, C., Bahl, C.R.H., Hansen, M.F.: Experimental and theoretical studies of nanoparticles of antiferromagnetic materials. J. Phys. Condens. Matter. **19**, 213202 (2007)

3. Kodama, R.H., Berkowitz, A.E.: Atomic-scale magnetic modeling of oxide nanoparticles. Phys. Rev. B. **59**, 6321–6336 (1999)

4. Millan, A., Urtizberea, A., Silva, N.J.O., Palacio, F., Amaral, V.S., Snoeck, E., Serin, V.: Surface effects in maghemite nanoparticles. J. Magn. Magn. Mater. **312**, L5–L9 (2007)

5. Kirillov, V.L., Balaev, D.A., Semenov, S.V., Shaikhutdinov, K.A., Martyanov, O.N.: Size control in the formation of magnetite nanoparticles in the presence of citrate ions. Mater. Chem. Phys. **145**, 75–81 (2014)

6. Néel, L., Acad, C.R.: Sci. Paris. **252**, 4075 (1961)

7. Makhlouf, S.A., Parker, F.T., Berkowitz, A.E.: Magnetic hysteresis anomalies in ferritin. Phys. Rev. B. **55**, R14717–R14720 (1997)

8. Seehra, M.S., Babu, V.S., Manivannan, A., Lynn, J.W.: Neutron scattering and magnetic studies of ferrihydrite nanoparticles. Phys. Rev. B. **61**, 3513–3518 (2000)

9. Punnoose, A., Phanthavady, T., Seehra, M.S., Shah, N., Huffman, G.P.: Magnetic properties of ferrihydrite nanoparticles doped with Ni, Mo, and Ir. Phys. Rev. B. **69**, 054425 (2004)

10. Gilles, C., Bonville, P., Rakoto, H., Broto, J.M., Wong, K.K.W., Mann, S.: Magnetic hysteresis and superantiferromagnetism in ferritin nanoparticles. J. Magn. Magn. Mater. **241**, 430–440 (2002)

11. Lepeshev, A.A., Karpov, I.V., Ushakov, A.V., Balaev, D.A., Krasikov, A.A., Dubrovskiy, A.A., Velikanov, D.A., Petrov, M.I.: Particularities of the magnetic state of CuO nanoparticles produced by low-pressure plasma arc discharge. J. Supercond. Nov. Magn. **30**, 931–936 (2017)

12. Balaev, D.A., Dubrovskii, A.A., Krasikov, A.A., Stolyar, S.V., Iskhakov, R.S., Ladygina, V.P., Khilazheva, E.D.: Mechanism of the formation of an uncompensated magnetic moment in bacterial ferrihydrite nanoparticles. JETP Lett. **98**, 139–142 (2013)

13. Balaev, D.A., Krasikov, A.A., Dubrovskii, A.A., Semenov, S.V., Bayukov, O.A., Stolyar, S.V., Iskhakov, R.S., Ladygina, V.P., Ishchenko, L.A.: Magnetic properties and the mechanism of formation of the uncompensated magnetic moment of antiferromagnetic ferrihydrite nanoparticles of a bacterial origin. J. Exp. Theor. Phys. **119**, 479–487 (2014)

14. Silva, N.J.O., Amaral, V.S., Urtizberea, A., Bustamante, R., Millán, A., Palacio, F., Kampert, E., Zeitler, U., de Brion, S., Iglesias, Ò., Labarta, A.: Shifted loops and coercivity from field-imprinted high-energy barriers in ferritin and ferrihydrite nanoparticles. Phys. Rev. B. **84**, 104427 (2011)

15. Silva, N.J.O., Amaral, V.S., Carlos, L.D.: Relevance of magnetic moment distribution and scaling law methods to study the magnetic behavior of antiferromagnetic nanoparticles: application to ferritin. Phys. Rev. B. **71**, 184408 (2005)

16. Michel, F.M., Ehm, L., Antao, S.M., Lee, P.L., Chupas, P.J., Liu, G., Strongin, D.R., Schoonen, M.A.A., Phillips, B.L., Parise, J.B.: The structure of ferrihydrite, a nanocrystalline material. Science **316**, 1726–1729 (2007)

17. Stolyar, S.V., Yaroslavtsev, R.N., Iskhakov, R.S., Bayukov, O.A., Balaev, D.A., Dubrovskii, A.A., Krasikov, A.A., Ladygina, V.P., Vorotynov, A.M., Volochaev, M.N.: Magnetic and resonance properties of ferrihydrite nanoparticles doped with cobalt. Phys. Solid State **59**, 555–563 (2017)

18. Stolyar, S.V., Bayukov, O.A., Gurevich, Y.L., Ladygina, V.P., Iskhakov, R.S., Pustoshilov, P.P.: Mössbauer study of bacterial ferrihydrite. Inorg. Mater. **43**, 638–641 (2007)

19. Raikher, Y.L., Stepanov, V.I., Stolyar, S.V., Ladygina, V.P., Balaev, D.A., Ishchenko, L.A., Balasoiu, M.: Magnetic properties of biomineral particles produced by bacteria Klebsiella oxytoca. Phys. Solid State **52**, 298–305 (2010)

20. Balaev, D.A., Krasikov, A.A., Dubrovskiy, A.A., Popkov, S.I., Stolyar, S.V., Bayukov, O.A., Iskhakov, R.S., Ladygina, V.P., Yaroslavtsev, R.N.: Magnetic properties of heat treated bacterial ferrihydrite nanoparticles. J. Magn. Magn. Mater. **410**, 171–180 (2016)

21. Balaev, D.A., Krasikov, A.A., Stolyar, S.V., Iskhakov, R.S., Ladygina, V.P., Yaroslavtsev, R.N., Bayukov, O.A., Vorotynov, A.M., Volochaev, M.N., Dubrovskiy, A.A.: Change in the magnetic properties of nanoferrihydrite with an increase in the volume of nanoparticles during low-temperature annealing. Phys. Solid State **58**, 1782–1791 (2016)

22. Stolyar, S.V., Bayukov, O.A., Ladygina, V.P., Iskhakov, R.S., Ishchenko, L.A., Yakovchuk, V.Y., Dobretsov, K.G., Pozdnyakov, A.I., Piksina, O.E.: Mössbauer investigation of temperature transformations in bacterial ferrihydrite. Phys. Solid State **53**, 100–104 (2011)

23. Stolyar, S.V., Balaev, D.A., Krasikov, A.A., Dubrovskiy, A.A., Yaroslavtsev, R.N., Bayukov, O.A., Volochaev, M.N., Iskhakov, R.S.: Modification of the structure and magnetic properties of cobalt-doped ferrihydrite nanoparticles under heat treatment. J. Supercond. Nov. Magn. **31**, 1133–1138 (2018)

24. Stoner, E.C., Wohlfarth, E.P.: A mechanism of magnetic hysteresis in heterogeneous alloys. Philos. Trans. R. Soc. A Math. Phys. Eng. Sci. **240**, 599–642 (1948)

25. Balaev, D.A., Krasikov, A.A., Dubrovskiy, A.A., Popkov, S.I., Stolyar, S.V., Iskhakov, R.S., Ladygina, V.P., Yaroslavtsev, R.N.: Exchange bias in nano-ferrihydrite. J. Appl. Phys. **120**, 183903 (2016)

26. Tüysüz, H., Salabaş, E.L., Weidenthaler, C., Schüth, F.: Synthesis and magnetic investigation of ordered mesoporous two-line ferrihydrite. J. Am. Chem. Soc. **130**, 280–287 (2008)

27. Bi, H., Li, S., Zhang, Y., Du, Y.: Ferromagnetic-like behavior of ultrafine NiO nanocrystallites. J. Magn. Magn. Mater. **277**, 363–367 (2004)

28. Makhlouf, S.A., Parker, F.T., Spada, F.E., Berkowitz, A.E.: Magnetic anomalies in NiO nanoparticles. J. Appl. Phys. **81**, 5561 (1997)

29. Makhlouf, S.A., Al-Attar, H., Kodama, R.H.: Particle size and temperature dependence of exchange bias in NiO nanoparticles. Solid State Commun. **145**, 1–4 (2008)

30. Seehra, M.S., Punnoose, A.: Particle size dependence of exchange-bias and coercivity in CuO nanoparticles. Solid State Commun. **128**, 299–302 (2003)

31. Díaz-Guerra, C., Vila, M., Piqueras, J.: Exchange bias in single-crystalline CuO nanowires. Appl. Phys. Lett. **96**, 193105 (2010)

32. Punnoose, A., Seehra, M.S.: Hysteresis anomalies and exchange bias in 6.6 nm CuO nanoparticles. J. Appl. Phys. **91**, 7766 (2002)

33. Punnoose, A., Magnone, H., Seehra, M.S., Bonevich, J.: Bulk to nanoscale magnetism and exchange bias in CuO nanoparticles. Phys. Rev. B. **64**, 174420 (2001)

34. Cooper, J.F.K., Ionescu, A., Langford, R.M., Ziebeck, K.R.A., Barnes, C.H.W., Gruar, R., Tighe, C., Darr, J.A., Thanh, N.T.K., Ouladdiaf, B.: Core/shell magnetism in NiO nanoparticles. J. Appl. Phys. **114**, 083906 (2013)

35. Bianchi, A.E., Stewart, S.J., Zysler, R.D., Punte, G.: Magnetic hardness features and loop shift in nanostructured CuO. J. Appl. Phys. **112**, 083904 (2012)

36. Bulte, J.W.M., Kraitchman, D.L.: Iron oxide MR contrast agents for molecular and cellular imaging. NMR Biomed. **17**, 484–499 (2004)

37. Inzhevatkin, E.V., Morozov, E.V., Khilazheva, E.D., Ladygina, V.P., Stolyar, S.V., Falaleev, O.V.: Elimination of iron-containing magnetic nanoparticles from the site of injection in mice: a magnetic-resonance imaging study. Bull. Exp. Biol. Med. **158**, 807–811 (2015)